Combined Theoretical and Experimental Deep-UV Resonance Raman Studies of Substituted Pyrenes

Johannes Neugebauer* and Evert Jan Baerends

Theoretical Chemistry, Vrije Universiteit Amsterdam, De Boelelaan 1083, 1081 HV Amsterdam, The Netherlands

Evtim V. Efremov,* Freek Ariese,* and Cees Gooijer

Analytical Chemistry & Applied Spectroscopy, Laser Centre, Vrije Universiteit Amsterdam, De Boelelaan 1083, 1081 HV Amsterdam, The Netherlands

Received: October 11, 2004; In Final Form: December 22, 2004

The results of time-dependent density functional theory (TDDFT) calculations of resonance Raman intensities are combined with experimental deep-ultraviolet resonance Raman measurements at a single wavelength, i.e., 244 nm, in order to test the possibility to distinguish several very similar compounds. Pyrene and three of its substituted derivatives, in which a single hydrogen atom has been replaced by a halogen atom, are compared. The fixed 244 nm excitation wavelength overlapped with the same electronic transition of the four pyrenes. Ground-state calculations using the BP86 exchange-correlation functional were used to predict the Raman frequencies, whereas excited-state calculations have been carried out employing the "statistical averaging of (model) orbital potentials" (SAOP) potential within a linear-response TDDFT framework in combination with the short-time approximation of resonance Raman intensities. In view of the simplistic theoretical approach, we find a surprisingly good agreement between the simulated and measured resonance Raman spectra of pyrene and its substituted analogues in terms of frequencies and intensities, which shows that the calculations can be used reliably to interpret the experimental spectra. With this combined information, it is possible to find criteria to distinguish the compounds under investigation, although many features of their vibrational spectra are similar.

1. Introduction

Resonance Raman spectroscopy (RRS) has evolved into an important tool in analytical chemistry during the past decades. In contrast to normal Raman scattering, it allows the detection of molecules with high sensitivity, since the Raman signal is enhanced by a factor of up to 10^6 when excitation into an absorption band of the molecule under study is applied (for reviews see, e.g., refs 1−3). RRS can also show enhanced selectivity because of the selective electronic excitation with tunable laser wavelengths: If complex samples are dealt with, only those compounds that are in resonance with the laser wavelength show enhanced Raman signals. In biopolymeric molecules RRS allows the selective study of the various chromophoric parts. Furthermore, since Raman scattering of water is very weak (in contrast to infrared spectroscopy) RRS will develop into an important tool for investigating biomolecules in an aqueous matrix.

RRS has become more and more important with the rapid progress in laser technology. The advent of continuous-wave (CW) ultraviolet (UV) lasers and the subsequent development of UV−RRS instrumentation[4−6] led to an extensive use of this technique.[7,8] Many molecules exhibit absorption maxima in the UV region and, rather unexpectedly, in the wavelength region below ≈260 nm, fluorescence background is very weak and does not overwhelm the spectra. UV−RRS was even successfully applied to highly fluorescent analytes, e.g., to mixtures of similar aromatic compounds.[9] This is particularly important for applications in the life sciences or in environmental research, where many of such strongly fluorescent impurities might be present. Even the type of vibration enhanced for a particular molecule can be varied by tuning the laser wavelength to different excitations.[10] Recently, it was shown that UV−RRS has reached a level of sensitivity that allows its on-line application in combination with column liquid chromatography[11] or capillary electrophoresis.[12] It should be noted, however, that, at present, tunability in the deep UV is still out of reach; only few laser lines are commonly available, the most important being 244 nm.

Working under resonance conditions increases sensitivity, but not all the vibrational modes will be present in the resonance-enhanced Raman spectrum; will this information still be sufficient for identification of similar compounds if there is no freedom of choice of excitation wavelength? Can excited-state calculations help us understand which vibrations are enhanced with a certain laser frequency? There are a number of questions regarding the use of RRS that require deeper fundamental understanding and theoretical research.

The calculation of resonance Raman spectra is, however, still a nonstandard procedure. A technique which is based on Kramers−Kronig relations between the polarizability tensor and the optical absorption was developed to calculate resonance Raman excitation profiles.[13−15] The corresponding "transform-theory" approach for the calculation of resonance Raman spectra[16] has been applied with some success during the past 10 years.[17−20] A recent study[20] showed that the progress in time-dependent density functional theory might help to increase the usefulness of this technique, although the results from the

* Corresponding authors. E-mail: jneugeb@chem.vu.nl; e.efremov@few.vu.nl; ariese@few.vu.nl

10.1021/jp045360d CCC: $30.25
Published on Web 02/17/2005

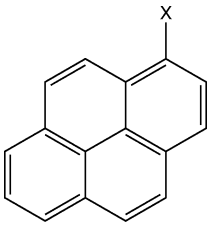

Figure 1. Lewis structures of pyrene (**1**, X = H) and substituted pyrenes (**2**, X = F; **3**, X = Cl; **4**, X = Br) investigated in this study.

simpler short-time approximation[1,21,22] were not much worse in that case. However, the transform theory requires the determination of excited-state minima, which might lead to problems, e.g., due to conical intersections.[23] Therefore, the estimation of resonance Raman intensities within the short-time approximation is still attractive to get qualitative insight into resonance Raman intensities.

Polycyclic aromatic hydrocarbons (PAH) are among the molecules most intensely studied by resonance Raman spectroscopy because they show very strong Raman scattering. They are also a potential health hazard, since many of them have the ability to induce cancer, so that their detection and identification is important in relation to occupational health and environmental pollution.[4,24] In this study we set out to combine experimental and theoretical efforts in order to investigate whether pyrene (**1**), one of the benchmark molecules within the PAH family, and the substituted pyrenes **2** to **4** in Figure 1, which differ only in one particular atom, can be distinguished reliably using RRS at a single excitation wavelength, i.e., at 244 nm. This set of molecules represents a "worst-case" approach in terms of identification, because all the analytes have practically identical vibrational modes. It should be noted that such a study presents a challenge bigger than analyzing substitutional isomers.

2. Computational Details

Density functional calculations have been performed using a modified version of the Amsterdam Density Functional (ADF) package.[25,26] The Becke-Perdew exchange-correlation functional, dubbed BP86,[27,28] was employed for ground-state structure optimization and frequency analysis. We used the SAOP potential (statistical averaging of (model) orbital potentials)[29−31] in combination with the TZP basis sets from the ADF basis set library[25] to calculate vertical excitation energies for structures displaced along the normal coordinates.

For the estimation of (relative) resonance Raman intensities, we used the short-time approximation for absorption and resonance Raman scattering (see, e.g., refs 1, 21, 22, 32, 33). In ref 20 it was shown that this approach can yield results comparable to more elaborate treatments based on excited-state structure optimizations.

Within the short-time approximation, the relative intensities i_j and i_k for modes j and k are given by[1,22]

$$\frac{i_j}{i_k} = \frac{\tilde{\nu}_j^2 \Delta_j^2}{\tilde{\nu}_k^2 \Delta_k^2} \qquad (1)$$

where $\tilde{\nu}_j$ or $\tilde{\nu}_j$ are the frequencies of vibration j and k, respectively, and Δ_j or Δ_k are displacements of the excited-state minimum along these modes in terms of dimensionless normal coordinates. These normal mode displacements are sometimes obtained by a fitting procedure of internal coordinate changes,[34] but within approximate treatments, they may also be calculated. Within the "independent mode, displaced harmonic oscillator" (IMDHO) model,[15,20] the relative intensities are equal to the square of the partial derivatives of the excited-state electronic energy $E_{\mathrm{el}}^{\mathrm{ex}}$ with respect to ground-state normal modes q_j at the ground-state equilibrium position,

$$\left(\frac{\partial E_{\mathrm{el}}^{\mathrm{ex}}}{\partial q_j}\right)_{q_j=0} = \tilde{\nu}_j(q_j - \Delta_j)|_{q_j=0} = -\tilde{\nu}_j\Delta_j \qquad (2)$$

and therefore they are calculated here by direct computation of the squares of the excited-state gradients, which is assumed to be a good approximation if only "short-time dynamics" of the nuclei are important.[1,35,36] We would like to point out that this is usually only a good approximation in the near-preresonance region and around the 0−0 line of a particular electronic transition.[37,38]

The derivatives are taken by numerical differentation of excitation energies for structures displaced along the normal coordinates of the molecule. Finite differences of excited-state energies are computed for states of the same electronic character as for the reference structure, which is identical to pure derivatives of adiabatic states if no couplings are present. In case of avoided crossings with small couplings, it means that these couplings are neglected. For large couplings, the Franck−Condon type approach used here will not be reliable. Within this approach, no explicit excited-state structure optimization is required. Since only relative intensities can be calculated, all intensities in this study are given in arbitrary units ("a.u."), and their absolute values do not have a meaning.

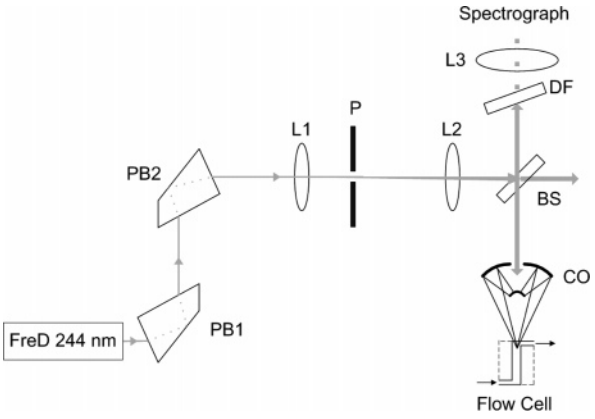

Figure 2. Experimental setup. FreD: frequency-doubled argon ion laser; PB: Pellin-Broca prism; L: lens; P: pinhole; CO: Cassegrain objective; BS: beam splitter; DF: dielectric stack filter. A detailed description of the setup is given in the text.

3. Experimental Section

Pyrene, 1-bromopyrene, and 1-chloropyrene were obtained from Sigma-Aldrich. 1-Fluoropyrene was purchased from Chiron (Trondheim, Norway). All analytes were dissolved in methanol (Fluka) with concentrations of 1 mg/mL. The absorption spectra of the analytes were measured with a Cary 50 absorption spectrometer using a 1-cm quartz cuvette.

A sketch of the setup of the UV−RRS system is shown in Figure 2. The light of an Innova FreD 90C (Coherent, Utrecht, The Netherlands) continuous frequency-doubled argon ion laser (wavelength: 244 nm, 40 mW) was projected on two Pellin-Broca prisms PB1 and PB2 (homemade), to remove the 488 nm fundamental laser line. The beam was then enlarged by a factor of 6 using a telescope consisting of two plano convex lenses L1 (focal length *f*, 50 mm) and L2 (*f*, 300 mm) and a pinhole, P. Via a beam splitter BS (model MUVBS45−FS-1D;

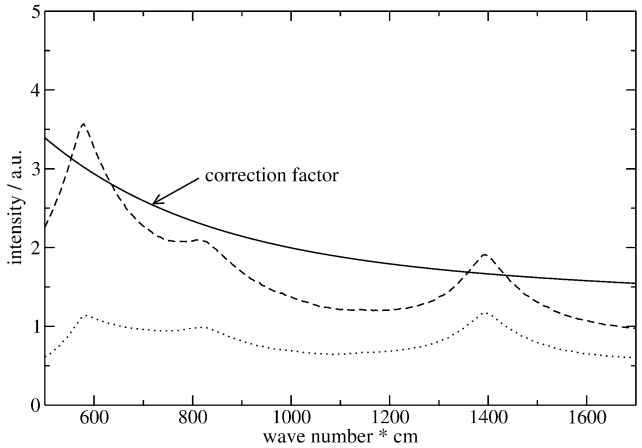

Figure 3. Spectra of a broadband Xenon flash lamp with (dotted line) and without (dashed line) the dielectric stack filter (DF in Figure 2). We shifted the wavenumber scale by the laser excitation frequency for better comparability to the experimental resonance Raman spectra. The solid line is an exponential fit to the ratio between the two curves, which is applied as a frequency-dependent correction factor to the resonance Raman spectra.

Acton Research) the laser light was projected onto a 25 × (NA: 0.4) Cassegrain objective CO (Ealing, Holliston, MA) and subsequently focused to a small spot inside a Z-shaped flow cell with an optical path length of 8 mm. The scattered light was then collected via the same objective (backscattering geometry). Removal of the laser line was achieved by using a dielectric stack filter DF (designed wavelength: 244 nm; Omega Optical, Brattleboro, VT). The filter properties depend on the orientation with respect to the light beam: While they are usually placed perpendicular to the beam, the cutoff wavelength can be optimized by varying their angle to the incident light. In our case effective rejection of the 244 nm light was achieved when the filter was turned 32 degrees. Of course, the transmission losses were not constant over the observed wavelength range. A correction profile was therefore applied to the spectra (see below). Finally the scattered light was projected via a focusing lens (*f*, 100 mm) to a single-stage 0.5-m spectrograph (Spex model 1870, Edison, NJ). The spectrograph had a grating of 1800 grooves/mm and a slit width of 70 μm, which resulted in a spectroscopic resolution (fwhm) of 15 cm^{-1}. The Raman spectra were recorded with a cooled (−20 °C) Andor Technology model DV420-OE CCD camera (Belfast, Northern Ireland). For spectral calibration, the spectrum of cyclohexane was used according to ref 39. The cell was connected to an LKB model 2150 pump (Pharmacia, Uppsala, Sweden) with a six-port injection valve equipped with a 200-μL injection loop. Methanol was used as carrier stream at a flow rate of 0.1 mL/min. These flow injection settings provided a recording window of ≈3 min and ensured that no photodegradation of the analytes occurred. All spectra were recorded for 100 s (five accumulations of 20 s each).

To compensate for the transmission function of the DF filter, a correction to the resonance Raman intensities had to be applied. The spectra of a broadband xenon flash lamp (IBH model 5000 XeF) were recorded with the filter (placed as described above) and without (see Figure 3). The ratio between these two spectra was calculated and then fitted with a first-order exponential function ($R_{sq} = 0.998$). The resulting wavelength-dependent correction factor, which is also shown in Figure 3, was applied to all measured spectra. In this paper, the most relevant frequency range from 500 to 1700 cm^{-1} will be shown.

TABLE 1: Calculated Vibrational Frequencies (BP86/TZP) in Units of cm^{-1} for Pyrene

no.	irrep	$\tilde{\nu}$	no.	irrep	$\tilde{\nu}$	no.	irrep	$\tilde{\nu}$
1	b_{1u}	99	25	a_{1g}	795	49	b_{2u}	1337
2	a_{1u}	146	26	b_{2u}	814	50	b_{1g}	1381
3	b_{1u}	206	27	b_{3g}	824	51	a_{1g}	1394
4	b_{2g}	244	28	b_{1u}	829	52	b_{1g}	1399
5	b_{3g}	255	29	a_{1u}	874	53	b_{2u}	1417
6	b_{3u}	348	30	b_{2g}	887	54	b_{2u}	1418
7	a_{1u}	392	31	b_{3g}	944	55	b_{2u}	1448
8	a_{1g}	402	32	a_{1u}	950	56	b_{2u}	1473
9	b_{1g}	453	33	b_{1u}	950	57	b_{1g}	1493
10	b_{1u}	486	34	b_{3g}	955	58	a_{1g}	1548
11	b_{2u}	492	35	b_{2u}	959	59	b_{1g}	1578
12	b_{1g}	493	36	b_{2u}	986	60	b_{2u}	1586
13	b_{3g}	502	37	a_{1g}	1060	61	b_{2u}	1595
14	b_{2g}	521	38	b_{2u}	1081	62	a_{1g}	1617
15	b_{2u}	541	39	b_{1g}	1100	63	b_{2u}	3085
16	b_{3g}	574	40	a_{1g}	1135	64	a_{1g}	3087
17	a_{1g}	584	41	b_{2u}	1141	65	b_{2u}	3087
18	a_{1u}	672	42	b_{1g}	1166	66	b_{1g}	3089
19	b_{2u}	687	43	b_{2u}	1167	67	b_{2u}	3094
20	b_{1u}	704	44	b_{2u}	1203	68	b_{1g}	3094
21	b_{1u}	729	45	b_{1g}	1227	69	a_{1g}	3106
22	b_{1g}	731	46	a_{1g}	1235	70	b_{2u}	3108
23	b_{3g}	758	47	b_{2u}	1236	71	b_{2u}	3113
24	b_{2g}	789	48	a_{1g}	1316	72	a_{1g}	3114

4. Calculated Vibrational Frequencies

The vibrational frequencies and normal modes of pyrene and the three substituted compounds 1-fluoropyrene, 1-chloropyrene, and 1-bromopyrene have been calculated using BP86/TZP. The full set of vibrational frequencies for the unsubstituted pyrene is shown in Table 1. It should be noted that according to group theory, only the totally symmetric irreducible representation can show nonvanishing electronic gradients for the excited states at the ground-state equilibrium structure for nondegenerate point groups. This was explicitly taken into account for the calculation of excited-state gradients. Whereas the unsubstituted compound is of D_{2h} symmetry and shows only 13 vibrations in the totally symmetric irrep a_{1g}, the substituted molecules are of the lower C_s symmetry, so that all vibrations corresponding to irreps a_{1g}, b_{1g}, b_{2u}, and b_{3u} for the D_{2h} symmetric compound now belong to the totally symmetric a′ irrep. In total, there are 49 symmetric modes for the substituted compounds; their vibrational frequencies are given in Tables S1, S2, and S3 in the Supporting Information.

The most obvious change in the vibrational frequencies is probably a missing high-frequency mode for the substituted pyrenes: for **1**, we find 10 different C−H stretch vibrations with wavenumbers >3000 cm^{-1}, while there are only 9 of these vibrations for the other molecules. The missing mode occurs in the low-frequency region of the spectra of the substituted compounds. From the normal modes obtained in the calculation it can be seen that there are C−X stretch vibrations at 881 cm^{-1} for X = F, at 824 cm^{-1} for X = Cl, and at 805 cm^{-1} for X = Br, for which no corresponding vibration, i.e., no vibration with a similar type of collective motion in pyrene can be found. Furthermore, there are characteristic low-frequency modes which involve a C−C−X angle bending, or a stretching of the C−X bond together with a squeezing of the aromatic ring to which the halogen atom is attached. The former appear at 251 cm^{-1} (F), 193 cm^{-1} (Cl), or 144 cm^{-1} (Br), while the latter can be found at 378 cm^{-1} (F), 325 cm^{-1} (Cl), or 238 cm^{-1} (Br). However, these vibrations are not useful for distinguishing the substituted compounds for two reasons: (i) they do not show significant resonance Raman intensities in our calculations, so that it might be difficult to use them for a discrimination of

TABLE 2: Experimental (E_{exp}) and Calculated (SAOP/TZP; E_{exp}) Vertical Excitation Energies for the Lowest Dipole-Allowed Transitions of Compounds 1 to 4

	state	E_{exp}/eV	E_{calc}/eV	E_{exp}/nm	E_{calc}/nm	f^a
pyrene (**1**)	$1B_{2u}$	3.72	3.38	333	367	0.208
	$1B_{3u}$	3.33	3.46	372	358	4.0*E*−5
	$2B_{3u}$	4.57	4.17	272	297	0.178
	$2B_{2u}$	5.18	5.07	239	245	0.573
1-fluoropyrene (**2**)	1A′	3.72	3.34	333	371	0.195
	4A′	4.56	4.14	272	299	0.165
	8A′	5.19	5.04	239	246	0.501
1-chloropyrene (**3**)	1A′	3.63	3.27	342	379	0.238
	4A′	4.51	4.09	275	303	0.175
	8A′		4.83		257	0.075
	9A′		4.97		249	0.251
	10A′		5.10		243	0.097
	11A′	5.14	5.11	241	243	0.160
1-bromopyrene (**4**)	1A′	3.61	3.24	343	383	0.244
	4A′	4.49	4.04	276	307	0.119
	9A′		4.84		256	0.091
	10A′	5.12	5.07	242	245	0.285
	11A′		5.09		244	0.177

[a] Calculated oscillator strengths (*f*). For the substituted pyrenes only excitations with oscillator strengths > 0.05 are given.

different compounds, and (ii) they could not be observed in practice because the filter transmission function becomes problematic in this wavenumber range (i.e., closer to the laser wavelength, see Figure 3).

The lowest-frequency modes that are important for the resonance Raman spectra can be found between 540 and 640 cm^{-1}. For the unsubstituted pyrene, there is only one totally symmetric mode in this range at 584 cm^{-1}, which can be described as a breathing mode of the aromatic rings. For the substituted compounds there are two vibrations in that frequency range. For 1-fluoropyrene, there is a collective angle bending mode in addition to the breathing mode, while these two vibrations mix for the heavier chlorine and bromine substituents. Among the higher-frequency modes, modes 37−39 involve a C−X stretch component, while modes 50, 51 and 59, 60 show a C−C−X angle bending contribution for all substituted pyrenes. Since some of these modes show a considerable intensity in the resonance Raman calculation, they will be discussed in more detail in section 6.

5. Electronic Transitions

To identify the electronic states which are in resonance with a certain laser excitation frequency, we calculated vertical excitation energies for pyrene and its substituted derivatives. The values for the lowest dipole-allowed excitations with considerable intensity are shown in Table 2 (for pyrene itself, all dipole-allowed states are listed; an extended list of excitation energies for all compounds is given in Tables S4−S7 in the Supporting Information). In this case, all singlet states within the irreps B_{1u}, B_{2u}, and B_{3u} are symmetry-allowed. Since the intensity of the resonance Raman bands depends on the fourth power of the transition dipole moment[20] to a certain electronic state, only states with a considerable oscillator strength will lead to intense resonance Raman scattering. For pyrene, the $2B_{2u}$ state at 245 nm (calculated; experimental value: 239 nm) has a high oscillator strength; the available 244 nm excitation wavelength is therefore very appropriate to conduct UV−RRS experiments.

All states are symmetry-allowed for the substituted compounds, although the *A″* states show a very low transition dipole moment. For 1-fluoropyrene, the 8*A′* state (calculated: 246 nm; experiment: 239 nm) will be most important for comparison with the resonance Raman experiments with excitation wavelength of 244 nm because of its high oscillator strength. 1-Chloropyrene is a bit more problematic, since there are three electronic states between 249 and 243 nm (calculated; experimental band maximum at 241 nm) with substantial oscillator strength, although none of them shows a calculated intensity comparable to the (calculated) 245/246 nm transitions of pyrene and 1-fluoropyrene. Also for 1-bromopyrene, we find two states at 245 and 244 nm (calculated; experimental band maximum at 242 nm) with relatively large oscillator strengths. All of these states might have to be considered for the resonance Raman intensities.

From the data in Table 2 it becomes obvious that the excitation energies for the two lower excited states with considerable intensity in experiment are underestimated by between 0.34 and 0.45 eV, while the discrepancy is smaller than 0.17 eV in all cases for the third intense experimental band. However, we are not focusing on the vertical excitation energies in this work, and other studies[40,41] have shown that the SAOP potential is well suited to describe properties depending on the shape of the excited-state potential energy surfaces, even though their vertical positions might be in error.

An analysis of the absorption spectrum of pyrene using TDDFT methods has recently been carried out.[42] Similar to the results obtained there, also our calculation reverses the order of the two lowest excited states: The intense $1B_{2u}$ ("L_a") state is 0.08 eV lower in energy than the weakly allowed $1B_{3u}$ ("L_b") state, while experimentally the L_b state is found at lower energy (3.33 eV). This underestimation of the $1B_{2u}$ state can be traced back to the problem of TDDFT in describing states with ionic character.[43]

6. Resonance Raman Spectra

Figure 4 shows a comparison of the calculated resonance Raman spectra of pyrene and 1-fluoropyrene and representations of some important vibrational normal modes. For pyrene, the gradient of the $2B_{2u}$ state (calc.: 245 nm) has been applied for the calculation of the resonance Raman intensities, while for 1-fluoropyrene the gradient of the 8*A′* state (calc.: 246 nm) has been used. Note that only relative intensities are calculated; therefore, the absolute values of the intensities do not have a physical meaning in our simulation.

The agreement between the calculation and experiment is remarkable in view of the simplistic ansatz in the theoretical approach: The peak positions and the relative intensities of almost all bands agree well between simulation and measurements. The good agreement of the peak positions, usually within 10 cm^{-1}, again demonstrates the reliability of the BP86 functional in frequency analyses if the calculated harmonic frequencies are directly compared to the experimental fundamental ones (i.e., without scaling of frequencies).[44−46] Additional comparisons to experimental infrared data[47] confirmed the good agreement for the vibrational frequencies.

As regards the relative intensities, the agreement of theoretical and experimental results is also very good, although there are some exceptions. The most important one is the band at 1548 (calc.; 1551 in experiment) or 1547 cm^{-1} (calc.; 1551 in experiment) for pyrene or 1-fluoropyrene, respectively, which is apparently too intense in the simulation. This is an angle bending mode, which for compound **2** (and also the other substituted pyrenes) also involves a bending of the X−C−C angles (X = F for compound **2**). A possible explanation for this disagreement would be a normal mode mixing between these vibrations and the vibrations at 1617 (pyrene) or 1618

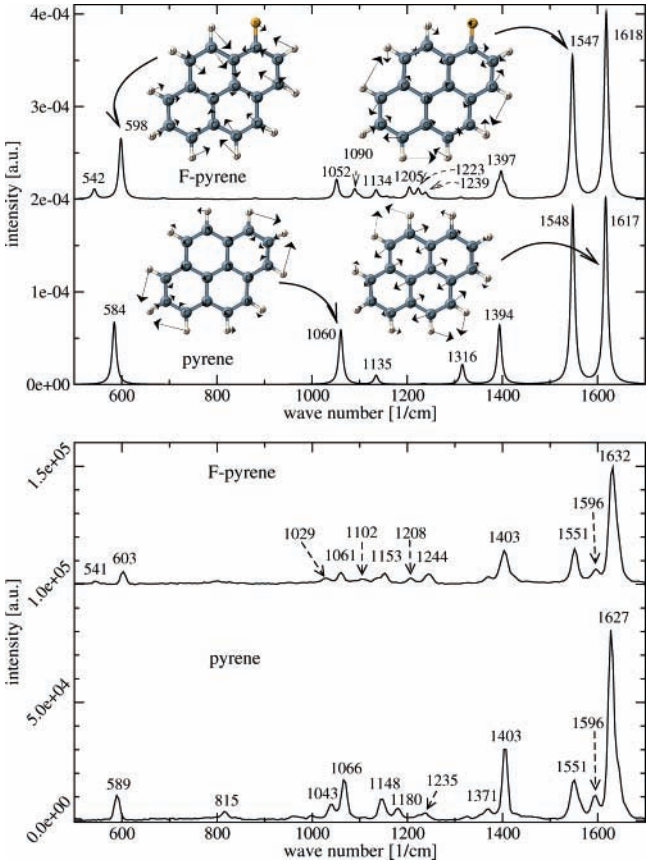

Figure 4. Comparison of calculated (top; SAOP/TZP) and experimental (λ_{ex} = 244 nm; bottom) resonance Raman spectra of pyrene and 1-fluoropyrene. Wavenumbers for the peaks are indicated in units of cm^{-1}.

cm^{-1} (1-fluoropyrene), which are of comparable frequency. It has been observed in refs 48 and 49 that such a Duschinsky rotation can affect the intensity calculation, and a comparison with intensities of combination bands of these two modes could help to clarify this point. Several bands of low intensity are present in the experimental resonance Raman spectrum around 3000 cm^{-1} (including C−H stretch fundamentals), so that it is not unambiguously possible to identify overtones and combination bands here. Also, the computational determination of overtone and combination band frequencies and intensities is beyond the scope of this work: Anharmonicities are not taken into account, but they are important for overtones and combination bands. Furthermore, the simple relationship in eq 1 holds only for fundamental transitions.

All the key features of the experiment are reproduced in the *first-principles* calculation: intense bands are found at 1617, 1548, 1394, 1060, and 584 cm^{-1} for pyrene and at 1618, 1547, 1397, and 598 cm^{-1} for 1-fluoropyrene in the simulation, while the most intense experimental peaks are found at 1627, 1551, 1403, 1066, and 589 cm^{-1} for pyrene, and at 1632, 1551, 1403, and 603 cm^{-1} for 1-fluoropyrene. The most intense band can be described as a distortion of the aromatic rings toward a rectangular shape, with additional contributions of H−C−C angle bendings.

As far as the differences between both compounds are concerned, we observe that in both the experimental and the calculated spectra the relative intensities of the peaks at about 1400 cm^{-1} (calculated values: 1394 for **1** and 1397 for **2**) and 1060 (calculated values: 1060 for **1** and 1052 for **2**) cm^{-1} decrease when going from pyrene to 1-fluoropyrene. In particular the latter peak involves a bending of the halogen atom for the substituted compounds, combined with an X−C stretch. The frequency shift for the "breathing mode" of the aromatic ring (calculated: at 584 cm^{-1} for pyrene and at 598 cm^{-1} for 1-fluoropyrene) is another important difference. The experimental values for these vibrations are 589 cm^{-1} (**1**) and 603 cm^{-1} (**2**), i.e., the experimental shift of 14 cm^{-1} for this band is very well reproduced in the calculation. An additional peak of very low intensity at 542 cm^{-1} can be found in our simulation for 1-fluoropyrene, which is also visible in the experiment (541 cm^{-1}).

Also the region between 1000 and 1300 cm^{-1} shows many differences between the two compounds. Several peaks of low intensity appear for 1-fluoropyrene, e.g, at 1052, 1090, 1134, 1205, 1223, and 1239 cm^{-1} in the simulation, similar to the experimental spectrum in this wavenumber range. However, there are also some additional experimental peaks for pyrene in this range, which are forbidden in the simulation, while the two most intense experimental peaks at 1066 and 1148 cm^{-1} also show up in the simulation (1060 and 1135 cm^{-1}). Possible reasons for the additional peaks could be Herzberg−Teller type scattering or overtones/combination bands, since these effects are not included in our approach to model resonance Raman spectra. Such bands can thus not appear in the simulation. Nevertheless, the overall picture for this wavenumber range is similar in simulation and experiment: There is one intense and clearly dominant peak at 1060 (calculated) or 1066 cm^{-1} (experimental) for pyrene, while several bands of smaller, but comparable intensity appear for 1-fluoropyrene.

As mentioned before, three different excited states (9A′, 10A′, and 11A′) with considerable oscillator strengths are obtained for 1-chloropyrene, which might be eligible for excitation by a 244 nm laser. Therefore, three separate simulations of the resonance Raman spectra have been performed. Since resonance Raman intensities depend on the fourth power of the transition dipole moment[20] of the electronic state in resonance, the intensities have been scaled by the ratios $(|\mu_A|/|\mu_B|)^4$, where μ_A and μ_B are the transition dipole moments for different excited states A and B; after scaling, the contribution of state 10A′ for 1-chloropyrene is negligible. The simulated spectra for the 9A′ and 11A′ states of 1-chloropyrene and for the 10A′ and 11A′ states of 1-bromopyrene are shown in Figure 5. We summed the scaled results for the different states to get the total spectra shown in Figure 6. It should be noted, however, that the most intense excitations, i.e., the contribution of state 9A′ (249 nm) for 1-chloropyrene and of state 10A′ (245 nm) for 1-bromopyrene dominate the final results.

Compared to the simulated spectra of pyrene and 1-fluoropyrene, there are now two intense peaks in the low-frequency range, at 576 and 632 cm^{-1} for 1-chloropyrene, while in the spectrum of 1-bromopyrene the lower-frequency peak (563 cm^{-1}) is less intense than the other one (606 cm^{-1}). The same intensity pattern can qualitatively be found experimentally, and also the agreement of the peak positions is remarkable: We obtain experimental values of 579 and 636 cm^{-1} for compound **3**, while the corresponding values for compound **4** are 570 and 617 cm^{-1}. The vibration at 1076 (**3**; calculated) or 1072 cm^{-1} (**4**; calculated) appears a bit more intense than the corresponding vibration in 1-fluoropyrene, which agrees with the experimental spectrum. The experimental frequencies for this vibration, which involves a X−C−C angle bending, are 1089 and 1084 cm^{-1} for **3** and **4**, respectively, compared to 1066 and 1061 cm^{-1} (experiment; calculated: 1060 and 1052 cm^{-1}) for **1** and **2**, respectively. Although the calculated peak positions do not

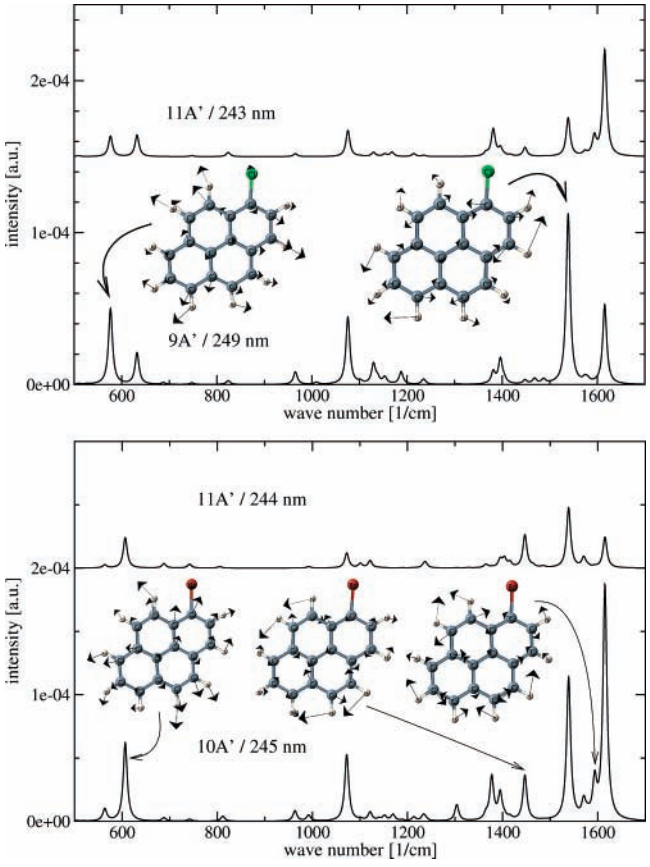

Figure 5. Calculated (SAOP/TZP) resonance Raman spectra of 1-chloropyrene (top) and 1-bromopyrene (bottom). Two different excited states are considered for both molecules. The intensities have been scaled according to the $|\mu|^4$ dependence of the resonance Raman intensities.

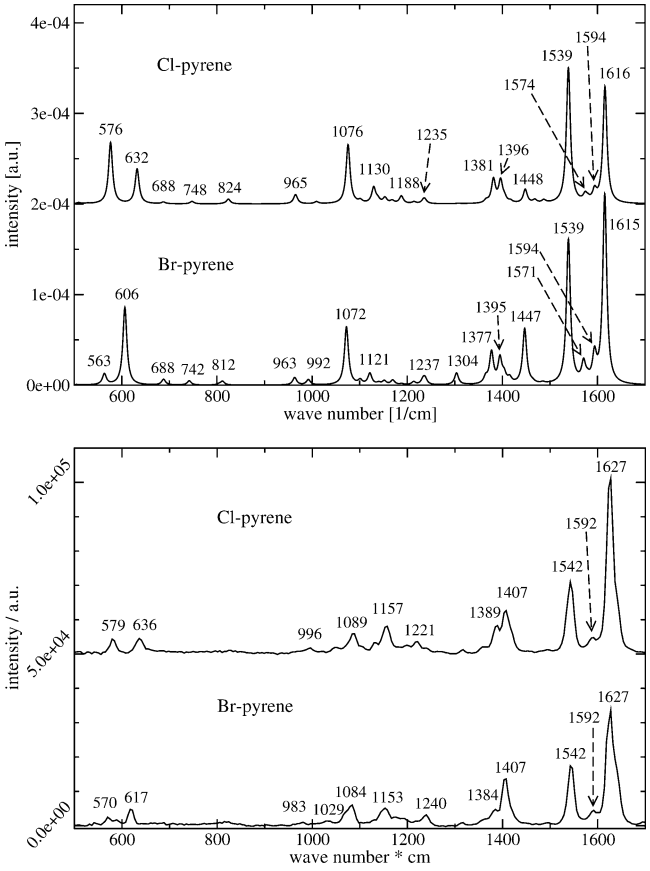

Figure 6. Comparison of calculated (top; SAOP/TZP) and experimental (λ_{ex} = 244 nm; bottom) resonance Raman spectra of 1-chloropyrene and 1-bromopyrene. For the calculated spectra the individual contributions shown in Figure 5 have been summed. Wavenumbers for the peaks are indicated in units of cm^{-1}.

exactly match the experimental ones, the accuracy of the differences for the different molecules is very good.

In the simulation for these two compounds, new peaks appear between the two highest-intensity modes at 1574 and 1594 cm^{-1} for **3**, and at 1571 and 1594 cm^{-1} for **4**. Their relative intensities are higher for 1-bromopyrene. In the experimental spectra, at least one of these two vibrations is visible, and the other one might be hidden below one of the other peaks. This peak is indeed a bit more intense for 1-bromopyrene, but it should be noted that similar peaks are also present in the experimental spectra for pyrene and 1-fluoropyrene, which are not reproduced in the simulation. Again, the most important discrepancy to the experiment is the somewhat too high intensity of the mode at 1539 (calculated; experiment: 1542) cm^{-1} for both compound **3** and **4**. Apparently the relative importance of the contribution from the 11A′ (**3**) and 10A′ state (**4**) is greater in the experimental spectra. This may be due to a more effective overlap of the true transition energy with the laser wavelength or a stronger oscillator strength than predicted by the calculation. Furthermore, we obtain peaks at 1448 cm^{-1} (1-chloropyrene) and 1447 cm^{-1} (1-bromopyrene) for which there is no corresponding vibration in the experimental spectra.

There is another important difference in the simulated spectra of 1-chloropyrene and 1-bromopyrene in comparison to the other two compounds: there are two peaks with considerable intensity around 1400 cm^{-1}, augmented with additional shoulders. They can be found at 1381 and 1396 cm^{-1} for 1-chloropyrene, and at 1377 and 1395 cm^{-1} for 1-bromopyrene. In the experimental spectra, there are also two peaks at 1389 and 1407 cm^{-1} for 1-chloropyrene, and at 1384 and 1407 cm^{-1} for 1-bromopyrene.

In the simulated spectra for compounds **1** and **2**, there is only one corresponding peak at 1394 cm^{-1} for **1** and at 1397 cm^{-1} for **2**, although it shows shoulders in case of 1-fluoropyrene. In the experimental spectra of compounds **1** and **2**, there is a second peak visible close to the peak at 1403 cm^{-1}, but it is of very small intensity.

From an analysis of the excited-state characters for structures displaced along the normal modes according to the scheme presented in ref 40 it could be seen that in case of 1-chloropyrene rather strong nonadiabatic couplings between the 10A′ and 11A′ occur. This mainly concerns the higher-frequency modes above 1350 cm^{-1}, and it is caused by the small energy gap between these states. Therefore, the estimates of resonance Raman intensities based on excited-state gradients will be less reliable for this molecule than for the others.

7. Conclusion

The first conclusion to be drawn from this study is that, despite the simplistic ansatz used for the theoretical description of the resonance Raman intensities, theoretical and experimental data agree to a large extent. This good agreement, which includes frequencies and intensities, allows us to perform an unambiguous assignment of the peaks in the experimental spectrum to theoretical data, and an interpretation in terms of the calculated normal modes of the system. The combined theoretical and experimental approach therefore yields a much more detailed insight into the resonance Raman measurements than pure experimental RRS can do, since it becomes im-

mediately clear which types of vibrations, i.e., which collective motions of the nuclei in the molecule are enhanced upon laser excitation.

Clearly, there are a lot of common features in the resonance Raman spectra for the selected compounds. But the systems chosen here can be considered a "worst-case" scenario for different reasons: The compounds under study differ only in one particular atom, so that many vibrational frequencies are approximately the same for all molecules. Furthermore, we restricted ourselves to a laser wavelength of 244 nm in the experimental part, which leads to a large enhancements of the Raman intensities for all compounds since they all show an absorption maximum close to this value. Unfortunately, this excitation does not considerably change the C−X bond character, so that no large differences for the different substituents X are induced. But despite these difficulties the combination of theoretical spectra simulation and experiment allows to clearly identify and interpret all differences in the spectra, so that several criteria for the discrimination between the different compounds could be found. In particular the low-frequency bands between 540 and 640 cm^{-1} show characteristic frequency and intensity patterns for each of the compounds. Also the (simulated) peak at 1060 cm^{-1} for pyrene and the corresponding vibrations for the other compounds, as well as the spectral features around 1400 cm^{-1} can help to identify the particular molecule under study. For many "real-life" applications larger differences can be expected than for the systems used here, so that experiment and theory can be a very powerful combination for this analytical technique.

Calculating intensities for several laser wavelengths, corresponding to different excited states of a particular compound at once opens up other possibilities for the combination of both approaches: In our study, this feature was applied to estimate the effect of a few close-lying excited states and to identify the state which is most likely in resonance with the laser line and contributing most to the experimental spectra (for 1-chloro- and 1-bromopyrene). It could also be employed to *predict* which excited states might be most appropriate to obtain different enhancements for similar compounds, making a discrimination between them much easier. In this way the calculation provides the possibility for an efficient prescreening of several transitions, one of which may then be selected for each compound. This would of course require that the experimental setup includes a tunable deep-UV laser source, so that all interesting transitions can be excited, and measurements are not restricted to a particular excitation wavelength. High repetition rate frequency-multiplied picosecond Ti:sapphire lasers may become quite appropriate for this purpose.[7]

Acknowledgment. J.N. gratefully acknowledges funding by a Forschungsstipendium of the Deutsche Forschungsgemeinschaft DFG. E.E. acknowledges financial support from FOM, project 00PFSI81.

Supporting Information Available: Calculated vibrational frequencies for compounds **2** to **4**. Lowest calculated vertical excitation energies for dipole-allowed transitions of compounds **1** to **4**. This material is available free of charge via the Internet at http://pubs.acs.org.

References and Notes

(1) Myers, A. B. *Chem. Rev.* **1996**, *96*, 911−926.

(2) Rousseau, D. L.; Friedman, J. M.; Williams, P. F. The Resonance Raman Effect. In *Raman Spectroscopy of Gases and Liquids*; Weber, A., Ed.; Springer: Berlin, 1979.

(3) Clark, R. J. H.; Steward, B. The Resonance Raman Effect. Review of the Theory and of Applications in Inorganic Chemistry. In *Structure and Bonding, Inorganic chemistry and spectroscopy*; Springer: Berlin, 1979.

(4) Asher, S. A. *Anal. Chem.* **1984**, *56*, 720−724.

(5) Asher, S. A. *Anal. Chem.* **1993**, *65*, 59A−66A.

(6) Asher, S. A. *Anal. Chem.* **1993**, *65*, 201A−210A.

(7) Austin, J. C.; Rodgers, K. R.; Spiro, T. G. Protein Structure from Ultraviolet Resonance Raman Spectroscopy. In *Metallobiochemistry, Part C: Spectroscopic and Physical Methods for Probing Metal Ion Environments in Metalloenzymes and Metalloproteins (Methods in Enzymology, Vol. 226)*; Riordan, J., Vallee, B., Eds.; Academic Press: New York, 1993.

(8) Haruta, N.; Aki, M.; Ozaki, S.; Watanabe, Y.; Kitagawa, T. *Biochemistry* **2001**, *40*, 6956−6963.

(9) Asher, S. A.; Johnson, C. R. *Science* **1984**, *225*, 311−313.

(10) Jones, C. M.; Asher, S. A. *J. Chem. Phys.* **1988**, *89*, 2649−2661.

(11) Dijkstra, R. J.; Martha, C. T.; Ariese, F.; Brinkman, U. A. T.; Gooijer, C. *Anal. Chem.* **2001**, *73*, 4977−4982.

(12) Dijkstra, R. J.; Efremov, E. V.; Ariese, F.; Brinkman, U. A. T.; Gooijer, C. *Anal. Chem.* **2003**, *75*, 5697−5702.

(13) Hizhnyakov, V.; Tehver, I. *Phys. Status Solidi* **1967**, *21*, 755−768.

(14) Tonks, D. L.; Page, J. B. *Chem. Phys. Lett.* **1979**, *66*, 449−453.

(15) Blazej, D. C.; Peticolas, W. L. *J. Chem. Phys.* **1980**, *72*, 3134−3142.

(16) Peticolas, W. L.; Rush, T., III *J. Comput. Chem.* **1995**, *16*, 1261−1270.

(17) Rush, T., III; Peticolas, W. L. *J. Phys. Chem.* **1995**, *99*, 14647−14658.

(18) Rush, T., III; Kumble, R.; Mukherjee, A.; Blackwood, M. E., Jr.; Spiro, T. G. *J. Phys. Chem.* **1996**, *100*, 12076−12085.

(19) Mroginski, M.-A.; Németh, K.; Magdó, I.; Müller, M.; Robben, U.; Védova, C. D.; Hildebrandt, P.; Mark, F. *J. Phys. Chem. B* **2000**, *104*, 10885−10899.

(20) Neugebauer, J.; Hess, B. A. *J. Chem. Phys.* **2004**, *120*, 11564−11577.

(21) Heller, E. J. *Acc. Chem. Res.* **1981**, *14*, 368−375.

(22) Heller, E. J.; Sundberg, R. L.; Tannor, D. *J. Phys. Chem.* **1982**, *86*, 1822−1833.

(23) Nooijen, M. *Int. J. Quantum Chem.* **2003**, *95*, 768−783.

(24) Brandt, H. C. A.; Watson, W. P. *Ann. Occup. Hyg.* **2003**, *47*, 349−378.

(25) "Amsterdam Density Functional program", Theoretical Chemistry, Vrije Universiteit, Amsterdam, URL: http://www.scm.com.

(26) te Velde, G.; Bickelhaupt, F. M.; Baerends, E. J.; van Gisbergen, S. J. A.; Guerra, C. F.; Snijders, J. G.; Ziegler, T. *J. Comput. Chem.* **2001**, *22*, 931−967.

(27) Becke, A. D. *Phys. Rev. A* **1988**, *38*, 3098−3100.

(28) Perdew, J. P. *Phys. Rev. B* **1986**, *33*, 8822−8824.

(29) Schipper, P. R. T.; Gritsenko, O. V.; van Gisbergen, S. J. A.; Baerends, E. J. *J. Chem. Phys.* **2000**, *112*, 1344−1352.

(30) Gritsenko, O. V.; Schipper, P. R. T.; Baerends, E. J. *Chem. Phys. Lett.* **1999**, *302*, 199−207.

(31) Gritsenko, O. V.; Schipper, P. R. T.; Baerends, E. J. *Int. J. Quantum Chem.* **2000**, *76*, 407−419.

(32) Myers, A. B. *Acc. Chem. Res.* **1997**, *30*, 519−527.

(33) Köppel, H.; Domcke, W.; Cederbaum, L. S. *Adv. Chem. Phys.* **1984**, *57*, 59.

(34) Dokter, A. M.; van Hemert, M. C.; 't Velt, C. M. I.; van der Hoef, K.; Lugtenburg, J. *J. Phys. Chem. A* **2002**, *106*, 9463−9469.

(35) Lee, S.-Y.; Heller, E. J. *J. Chem. Phys.* **1979**, *71*, 4777−4788.

(36) Markham, L. M.; Hudson, B. S. *J. Phys. Chem.* **1996**, *100*, 2731−2737.

(37) Siebrand, W.; Zgierski, M. Z. In *Excited States*, Vol. 4; Lim, E. C., Ed.; Academic Press: New York, 1979.

(38) Zerbetto, F.; Zgierski, M. Z. *J. Chem. Phys.* **1994**, *101*, 1842−1851.

(39) Fountain, A. W.; Vickers, T. J.; Mann, C. K. *Appl. Spectrosc.* **1998**, *52*, 462−468.

(40) Neugebauer, J.; Baerends, E. J.; Nooijen, M. *J. Chem. Phys.* **2004**, *121*, 6155−6166.

(41) Neugebauer, J.; Baerends, E. J.; Nooijen, M. *J. Phys. Chem. A* **2005**, *109*, 1168−1179.

(42) Dierksen, M.; Grimme, S. *J. Chem. Phys.* **2004**, *120*, 3544−3554.

(43) Grimme, S.; Parac, M. *Chem. Phys. Chem.* **2003**, *4*, 292−295.

(44) Neugebauer, J.; Hess, B. A. *J. Chem. Phys.* **2003**, *118*, 7215−7225.

(45) Reiher, M.; Neugebauer, J.; Hess, B. A. *Z. Physik. Chem.* **2003**, *217*, 91−103.

(46) Reiher, M.; Brehm, G.; Schneider, S. *J. Phys. Chem. A* **2004**, *108*, 734−742.

(47) National Institute of Standards and Technology, "NIST Chemistry WebBook", http://webbook.nist.gov/, 2004.

(48) Zgierski, M. Z. *Chem. Phys.* **1986**, *108*, 61−68.

(49) Zgierski, M. Z. *Chem. Phys. Lett.* **1987**, *136*, 252−257.